

# Anisotropic properties of spherical single crystals of $\text{La}_{1.8}\text{Sr}_{0.2}\text{CuO}_{4-\delta}$

A. Gardchareon<sup>a,b</sup> N. Mangkorntong<sup>b</sup> D. Hérisson<sup>a</sup>  
P. Nordblad<sup>a</sup>

<sup>a</sup>*Department of Engineering Sciences, Uppsala University, Box 534, SE-751 21 Uppsala, Sweden*

<sup>b</sup>*Faculty of Sciences, Chiang Mai University, Chiang Mai 50200, Thailand*

---

## Abstract

Single crystals of  $\text{La}_{1.8}\text{Sr}_{0.2}\text{CuO}_{4-\delta}$  grown by the travelling solvent floating zone method have been ground to spherical shape for studies of anisotropic superconducting properties by SQUID magnetometry. Here we report on magnetization measurements parallel and perpendicular to the  $c$ -axis on two of these crystals. At low enough temperatures and fields the spheres are perfectly shielding (susceptibility  $-1.5$  [SI]) and thus magnetically isotropic. The field dependence of the critical temperature, the transition width and the field expulsion well below  $T_c$  is qualitatively similar in both samples and is detailed in the paper. The anisotropy of the first critical field also shows similar behavior for the two crystals. Magnetization vs field experiments reveal a large difference in the hysteresis behavior along the two directions and an enhancement of the critical current density through the  $\text{CuO}_2$ -planes compared to the in-plane current density at higher fields.

*Key words:* Magnetic properties, Type II superconductor, High  $T_c$  superconductor, Anisotropy,  $\text{La}_{2-x}\text{Sr}_x\text{CuO}_{4-\delta}$   
*PACS:* 74.25.Qt, 74.72.Dn, 75.30.Gw

---

## 1 Introduction

$\text{La}_{2-x}\text{Sr}_x\text{CuO}_{4-\delta}$  is a high- $T_c$  superconducting compound (1; 2; 3) with a crystal structure that contains only one  $\text{CuO}_2$  plane per primitive cell. The superconductivity of the compound depends strongly on the Sr concentration (2; 3) and the physical properties of the system have been quite extensively investigated (4; 5; 6; 7; 8; 9; 10; 11; 12; 13; 14; 15; 16; 17; 18; 19) Here we report results from magnetization measurements parallel and perpendicular to

the *c*-axis of two spherical single crystal of nominally the same composition  $\text{La}_{1.8}\text{Sr}_{0.2}\text{CuO}_{4-\delta}$  (LSCO) still with quantitatively dissimilar properties.

One purpose of the study is to investigate the anisotropy of the magnetic response of an extreme type II superconducting system without any disturbing geometrical anisotropy at the moment of field penetration. Another objective of the study is to make a detailed mapping of the superconductivity of  $\text{La}_{2-x}\text{Sr}_x\text{CuO}_{4-\delta}$  as to the generality of the magnetic response and the anisotropy for two samples of nominally the same quality and composition.

## 2 Experimental details

### 2.1 Single Crystal Growth

The single crystals of  $\text{La}_{2-x}\text{Sr}_x\text{CuO}_{4-\delta}$  were prepared by means of the traveling solvent floating zone (TSFZ) method (20) using an optical image furnace of 4 cups type. The starting material was prepared by a solid state reaction from high purity (4N) powders of  $\text{La}_2\text{O}_3$ ,  $\text{SrCO}_3$  and  $\text{CuO}$ , formed into a powder rod by means of water press and sintered in air at  $1260^\circ\text{C}$  for 12 hr. To start the crystal growth, a powder rod was hanged inside a fused quartz tube, with the lower end of the rod slightly above a single crystal seed and at the focal point of an optical image furnace. Oxygen at a slightly higher than ambient pressure was admitted to flow through the quartz tube. A melting zone was created at the lower end of the rod by the heat generated from a set of four 300 watt halogen lamps. In order to lower the melting point, a piece of  $\text{CuO}$ , was employed as solvent. The crystal seed was moved up and connected to the melting zone of the powder rod to initiate the growth of the single crystal. The powder rod and the single crystal seed were rotated in opposite directions at a speed of 15 – 30 rpm. Then they were slowly moved downward together at a rate of about 0.8 mm/hr while the melting zone remained at the focus of the lamp images causing the lower part of the rod to become a solid single crystal. This process was carried out until a complete single crystal rod had been formed. Typical dimensions of the single crystal rods were 8 – 10 cm of length and 4 – 6 mm in diameter. The crystal rods were always annealed in one atm of oxygen, at  $800^\circ\text{C}$  for 240 hours prior to any characterization.

A powder X-ray diffraction pattern of a sample extracted from one of the LSCO crystals is shown in Fig. 1. It shows that this sample is single phased without noticeable impurities ( $\leq 0.5\%$ ). Composition analyses of several single crystal rods were carried out by means of an Electron Probe Microanalyzer instrument (JEOL EPMA), which revealed that the composition of the LSCO crystals was homogeneous and uniform throughout the length of the rods. Sin-

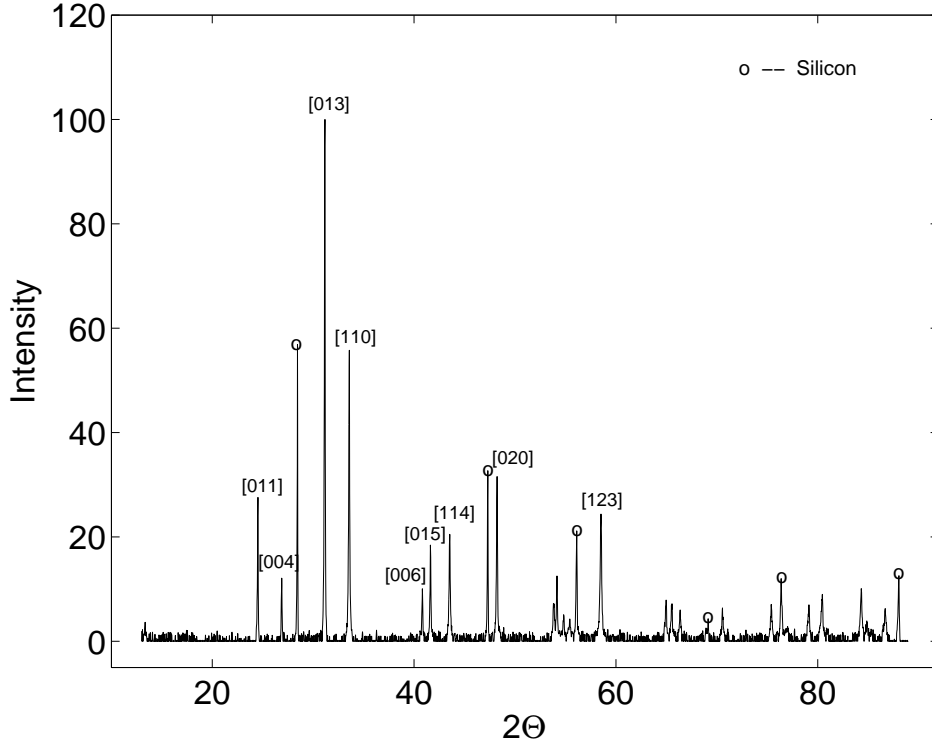


Fig. 1. A powder x-ray diffraction pattern of a LSCO sample. The strongest LSCO peaks are labelled and the Si peaks marked by circles.  $\lambda = 1.5406 \text{ \AA}$ .

gle domain examination was done by a metallurgical optical microscope and Laue photography. From these characterization results the single crystals were found to be of high quality. Some special properties of these LSCO crystals have been studied with neutron scattering (7).

Two single crystal rods of  $\text{La}_{1.8}\text{Sr}_{0.2}\text{CuO}_{4-\delta}$  were selected for further studies. It was found from powder x-ray diffraction measurement that these two samples have tetragonal structure with  $a = 3.7738 \pm 0.0001 \text{ \AA}$ ,  $c = 13.2467 \pm 0.0008 \text{ \AA}$  for the first crystal (sample 1) and  $a = 3.7719 \pm 0.0001 \text{ \AA}$ ,  $c = 13.2528 \pm 0.0007 \text{ \AA}$  for the second crystal (sample 2). Comparing these parameters to the relation between Sr content  $x$  and the lattice constants at room temperature reported by Takagi et al.(21), the Sr content  $x$  for our samples was confirmed to be close to the nominal  $x \approx 0.2$ . The transition temperatures ( $T_c$ ) of the two crystals were found to be 30.5 K and 33.5 K for sample 1 and sample 2, respectively.

## 2.2 Experimental procedures

Spherical single crystal samples were ground from the two single crystal rods. Pieces of about 4 mm of length were cut from the rods by a diamond saw. The pieces were first hand ground and then ground to good spherical shape in a special sphere grinding tool. The diameter of the two spheres employed in this

study is about 2 mm, and the mass of the crystals are 28.90 mg (sample 1) and 30.80 mg (sample 2), respectively. The c-axis directions of the spheres were determined (and clearly marked) by using the single crystal diffractometer (SXD) at the Studsvik Neutron Research Laboratory, Sweden.

A commercial SQUID magnetometer (Quantum Design MPMSXL) with a 5 T magnet was used to measure the magnetic properties of the samples. The temperature dependence of zero-field-cooled (ZFC), field-cooled (FC) and thermoremanent (TRM) magnetization was measured in the temperature range 5 – 40 K with the magnetic field applied parallel and perpendicular to the c-axis of the samples. The measurements were performed in different applied magnetic fields ranging between 0.08 and 40 kA/m. The field dependence of the magnetization (full hysteresis curves) of the two samples in fields up to  $4 \times 10^3$  kA/m was measured at different constant temperatures and with the field applied parallel and perpendicular to the c-axis of the samples.

The zero-field-cooled magnetization ( $M_{ZFC}$ ) is obtained by cooling the sample to a temperature below the transition temperature  $T_c$  in the absence of the field, turning on an applied magnetic field, and measuring the magnetization in this field as the sample warms through  $T_c$ . The field-cooled-cooling magnetization ( $M_{FC}$ ) is obtained by cooling the sample in an applied magnetic field and measuring the magnetization in this field as the sample is cooled. All FC results of this paper are recorded on cooling, however, for comparison, some FC-magnetization were also recorded on re-heating the sample; these data did not deviate significantly from the cooling results. The thermo-remanent-magnetization ( $M_{TRM}$ ) is obtained by turning off the field after field-cooling and measure the magnetization as the sample is reheated through  $T_c$ .

### 3 Results and discussion

#### 3.1 Temperature dependence of the magnetization

The crystals were first investigated by recording the temperature dependence of the magnetization at different applied fields along the two principal axes of the samples using the ZFC, FC and TRM protocols as described above. From the low field  $M$  vs  $T$  curves the transition temperatures of the two samples were determined to be 30.5 K and 33.5 K for sample 1 and 2, respectively. ( $T_c$  is here defined from the temperature for the onset of a diamagnetic signal in the ZFC and FC magnetization curves.)

Fig. 2 TOP shows  $M/H$  vs  $T$  at different applied fields for sample 1 with the

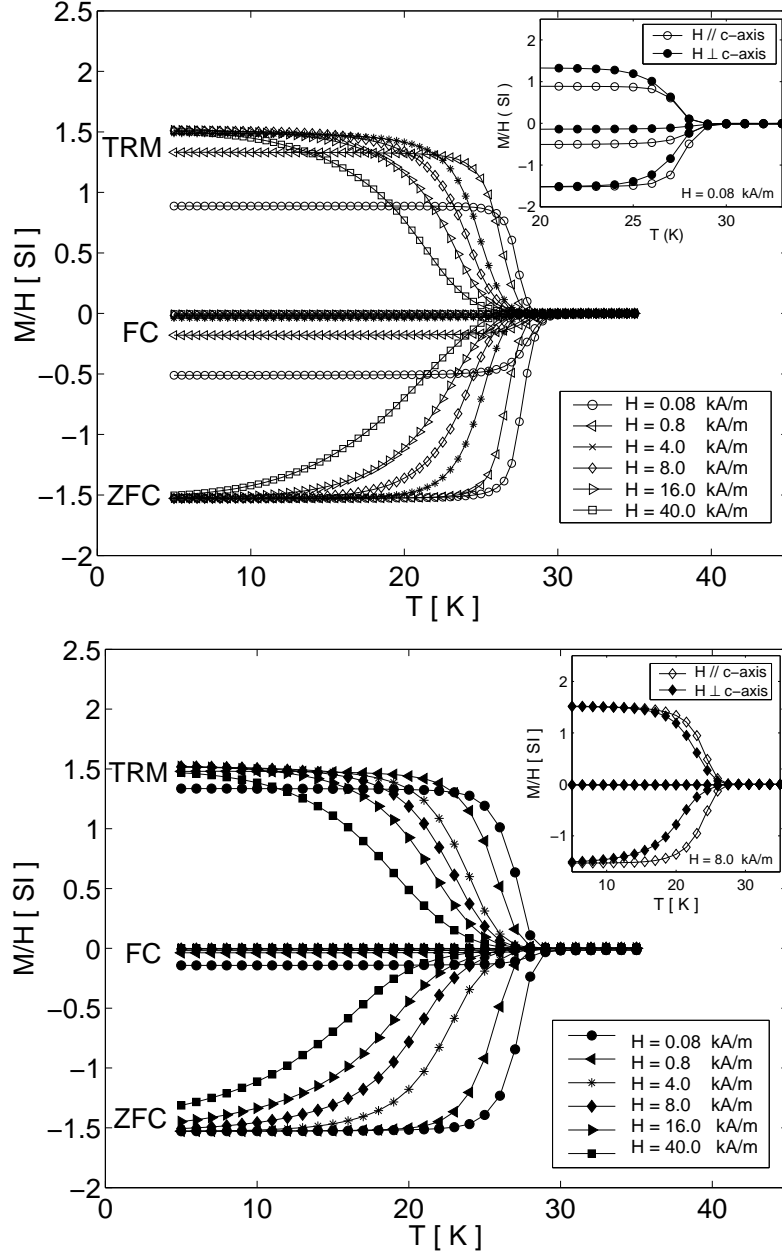


Fig. 2. Temperature dependence of the ZFC, FC and TRM “susceptibility” ( $M/H$ , [SI]) for the field parallel (TOP) or perpendicular (BOTTOM) to the  $c$ -axis of sample 1,  $H = 0.08, 0.8, 4.0, 8.0, 16.0$  and  $40.0$  kA/m. The insets show the temperature dependence of the ZFC, FC and TRM “susceptibility” for the field parallel and perpendicular to the  $c$ -axis, for  $H = 0.08$  kA/m (TOP) and  $H = 8.0$  kA/m (BOTTOM).

field applied along the  $c$ -axis. It should be noted that the value of  $M_{ZFC}/H = -1.5$  at low temperatures corresponds to the perfect shielding value for a superconductor of spherical shape ( $\chi = -\frac{1}{1-N}$ , where  $N = \frac{1}{3}$  is the demagnetising factor, leads to  $\chi = -1.5$ ). As is seen from the figure the field expulsion ( $M_{FC}/H$ ), on the other hand, is quite weak and rapidly decreasing with increasing field.

Fig. 2 BOTTOM shows  $M/H$  vs  $T$  at different applied fields for sample 1 with the field applied perpendicular to the  $c$ -axis. The low temperature value of  $M_{\text{ZFC}}/H = -1.5$ , corresponds to perfect shielding as when the field is applied parallel to the  $c$ -axis. The field expulsion in this case is even weaker than when the field is applied parallel to the  $c$ -axis.

The insets of Fig. 2 give a comparison between the behavior of  $M/H$  for  $H$  parallel and perpendicular to the  $c$ -axis at a weak field,  $H = 0.08$  kA/m (TOP inset) and a somewhat stronger field  $H = 8.0$  kA/m (BOTTOM inset). It is clearly seen from the figure that  $M/H$  is more strongly suppressed by the field when the field is applied perpendicular to the  $c$ -axis, i.e., when the induced supercurrents must travel through the areas linking the superconducting  $\text{CuO}_2$ -planes.

The corresponding curves for sample 2 give a qualitatively similar picture as Fig. 2 for sample 1, however with some quantitative differences, which we will discuss below.

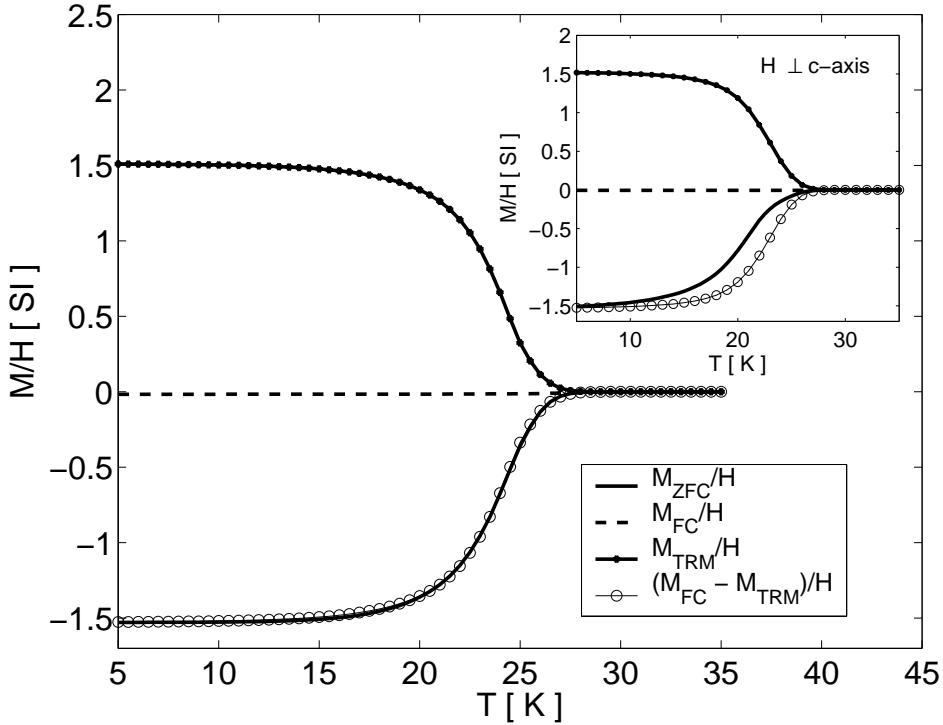


Fig. 3. Temperature dependence of the ZFC, FC and TRM “susceptibility” for the field parallel to the  $c$ -axis of sample 1 ( $H = 8.0$  kA/m), the open squares represent  $M_{\text{FC}} - M_{\text{TRM}}$ , which is indistinguishable from  $M_{\text{ZFC}}$  and confirms the validity of the principle of superposition. The inset shows the corresponding curves when the 8.0 kA/m field is applied perpendicular to the  $c$ -axis and shows that the principal of superposition is no longer valid.

The fundamental relation  $M_{\text{ZFC}} = M_{\text{FC}} - M_{\text{TRM}}$ , which is based upon the principle of superposition and only valid for a system that yields linear re-

sponse to a field change, is found to apply for low fields, but to be violated for higher fields. The relation is valid up to higher magnetic fields applied parallel to the  $c$ -axis than perpendicular to the  $c$ -axis as can be seen in Fig. 3, where  $M_{ZFC} = M_{FC} - M_{TRM}$  data for an applied field of 8.0 kA/m applied parallel (main frame) and perpendicular to the  $c$ -axis (inset) are shown for sample 1. The validity of the relation is only certified when the sample is able to fully shield a field change, i.e., when there is no further field penetration. Additionally, the trapped field from the field cooled process must remain trapped when the field is removed for the measurement of the TRM state. The two samples show very similar behavior as to the applicability of the principle of superposition.

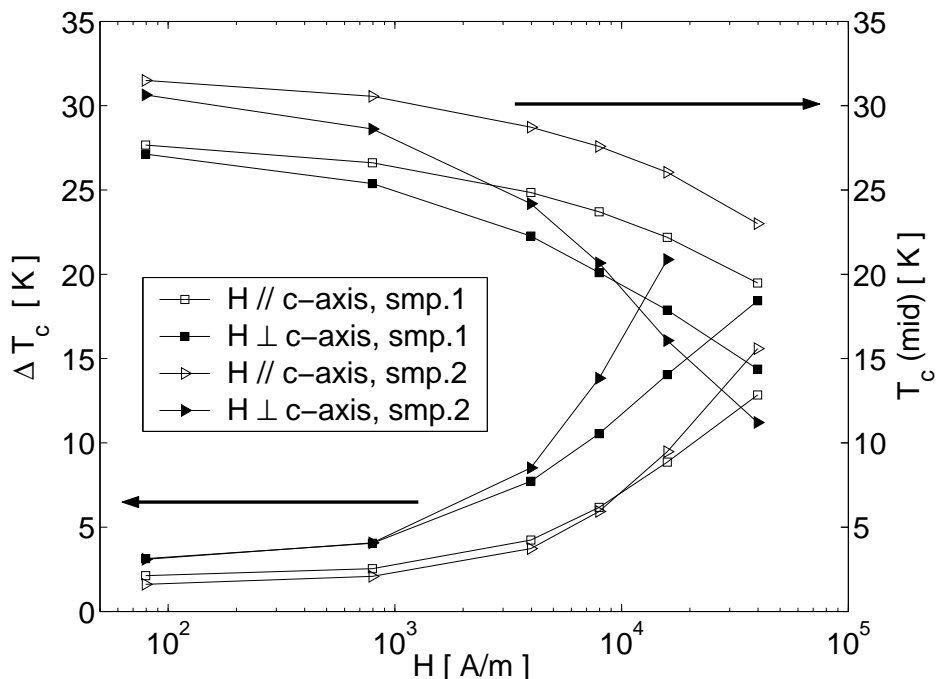


Fig. 4. Field dependence (logarithmic scale) of  $\Delta T_c$  and  $T_c(\text{mid})$  for the magnetic field applied parallel and perpendicular to the  $c$ -axis for sample 1 and sample 2.

An important consequence of an increasing applied magnetic field on a high temperature superconductor is that the superconducting temperature is lowered and that the width of the transition increases. Fig. 4 illustrates the increase of the width of the transition  $\Delta T_c$ , defined from the difference between the temperatures for which the shielding has reached 10% and 90% of the full shielding level, and the decrease of  $T_c(\text{mid})$ , here defined through the temperature where half of full shielding is measured. The change of the parameters is plotted vs. applied magnetic field for both samples and with the field applied parallel and perpendicular to the  $c$ -axis. The figure shows that the increase of  $\Delta T_c$  and the decrease of  $T_c(\text{mid})$  is much stronger for magnetic fields perpendicular to the  $c$ -axis than for magnetic fields parallel to the  $c$ -axis and again that the behavior of the two samples is similar. However, a somewhat stronger

field dependence for the sample with the higher  $T_c$  (sample 2) can be noticed. It should be mentioned that the decrease of  $T_c(\text{mid})$  with the field is stronger than the decrease of  $T_c$  onset.

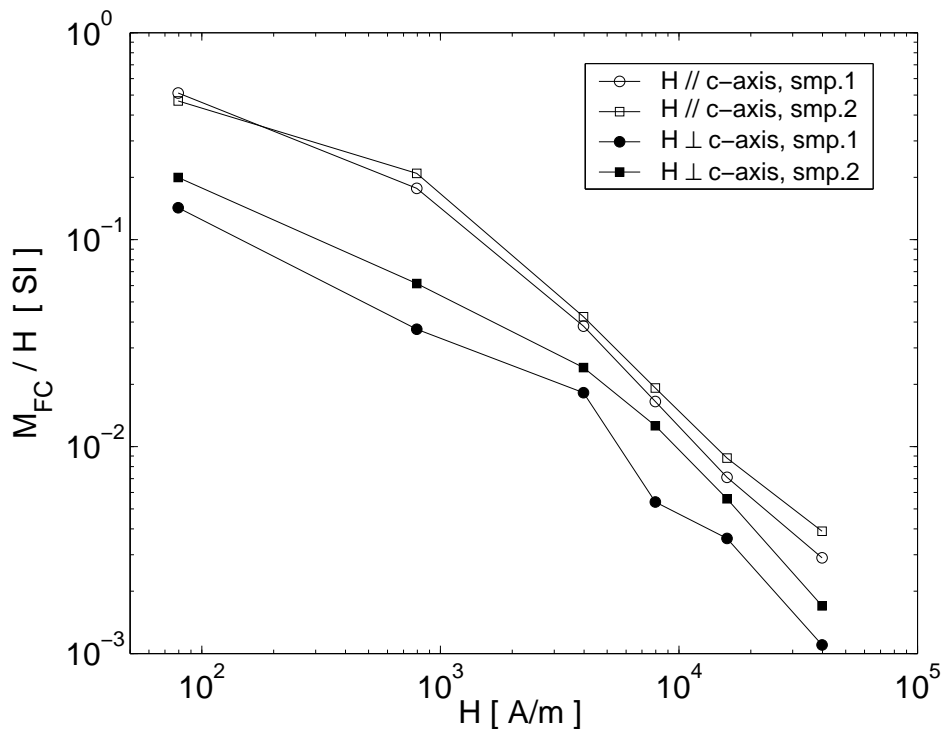


Fig. 5. Field dependence of the low temperature field cooled “susceptibility” ( $M_{\text{FC}}/H$ ) (temperature independent at low enough temperatures), when the field is applied parallel and perpendicular to the c-axis of sample 1 and sample 2.

Fig. 5 shows the field dependence of the magnitude of the field expulsion ( $M_{\text{FC}}$ ) of sample 1 and 2 for applied magnetic fields parallel and perpendicular to the c-axis. The magnitude of  $M_{\text{FC}}$  for applied magnetic fields parallel to the c-axis is higher than for fields applied perpendicular to the c-axis. The field expulsion is quite weak, at a field of 0.08 kA/m it amounts to  $\sim 30\%$  of complete field expulsion for fields parallel to the c-axis, but only  $\sim 10\%$  for fields perpendicular to the c-axis for both samples and it is rapidly decreasing with increasing field. The small value of the flux expulsion even at quite weak fields implies that the flux lines are always strongly trapped in these samples.

### 3.2 Field dependence of the magnetization

The upper graph of Fig. 6 shows the field dependence of the magnetization in the field range -800 kA/m to 800 kA/m at four different temperatures in the range  $T/T_c = 0.175 - 0.702$ , when the field is applied parallel to the c-axis for sample 1 (sample 2 shows a similar behavior). It is seen that the hysteresis



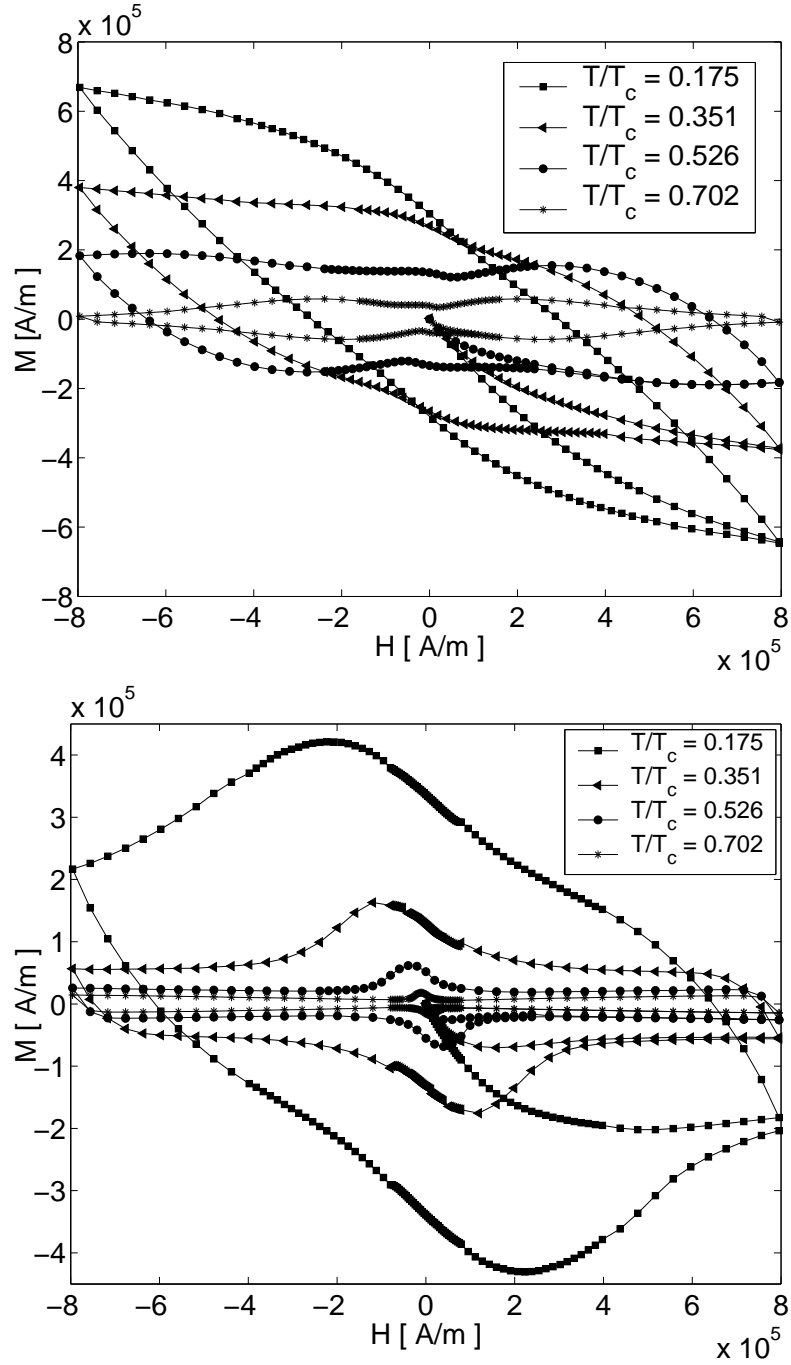


Fig. 6. Field dependence of magnetization at  $T/T_c = 0.175, 0.351, 0.526$  and  $0.702$  for magnetic fields applied parallel (TOP) and perpendicular (BOTTOM) to the  $c$ -axis of sample 1.

loop becomes more narrow with increasing temperature, a direct reflection of the decrease of the first critical field ( $H_{c1}$ ) and the critical current density ( $J_c$ ) of the samples with increasing temperature. One also notices that the field for full flux penetration (the minimum in the virgin  $M$  vs  $H$  curve) is not reached in these experiments at the two lower temperatures.

The lower part of Fig. 6 shows the corresponding  $M$  vs  $H$  curves when the field is applied perpendicular to the  $c$ -axis of sample 1 (a similar behavior is observed for sample 2). The width of the hysteresis loop is significantly smaller than when magnetic field is applied parallel to the  $c$ -axis and the field for full flux penetration is reached at all the measured temperatures.

Some features of these hysteresis loops are worth to note: The initial slope of all curves corresponds to perfect shielding i.e.  $M/H = -1.5$ , the curves start to deviate from this straight line at a quite well defined field value, the effective first critical field ( $H_{c1eff} = H_{c1}/1.5$ ), and the continued  $M$  vs  $H$  loop for the different directions imply that there are strongly temperature and directional dependent pinning forces and critical currents in the samples.

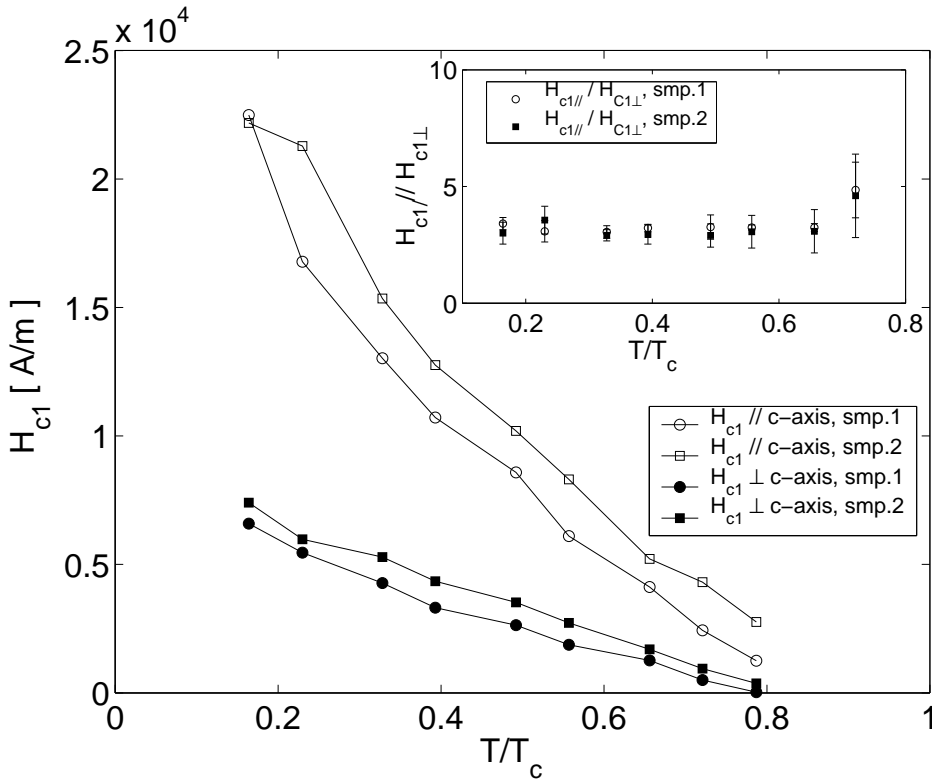


Fig. 7.  $H$ - $T$  phase diagram showing  $H_{c1}$  vs  $T/T_c$  for the two samples both parallel and perpendicular to the  $c$ -axis. The inset shows the calculated anisotropy of  $H_{c1}$  ( $H_{c1\parallel}/H_{c1\perp}$ ) for the two samples.

Using the low field initial curves of Fig. 6 and the corresponding curves for sample 2, we can derive estimates of the first critical field of the samples. In Fig. 7,  $H_{c1}$  is plotted vs temperature ( $T/T_c$ ) for both field directions and for the two samples. In the inset the anisotropy of the first critical field defined from ( $H_{c1\parallel}/H_{c1\perp}$ ) is shown. The first critical field  $H_{c1}$  is found to increase almost linearly on decreasing temperature and to show an anisotropy independent of temperature as shown by the inset of Fig. 7. The average value of the  $H_{c1}$ -anisotropy, weighted by errorbars, is found to be  $3.1 \pm 0.1$ . The measured

data of the field dependence of  $H_{c1}$  is somewhat scattered, but it is a great advantage to use a spherical single crystal to study the behaviour of the first critical field of a highly anisotropic superconductor, since geometrical factors are effectively avoided.

In a standard Ginzburg-Landau Model of supraconductivity (22; 23),  $H_{c1}$  is related to the order parameter coherence length  $\xi$  and the field penetration depth  $\lambda$  with a good approximation through (24):

$$\mu_0 H_{c1} = \frac{\Phi_0}{4\pi\lambda^2} (\ln(\lambda/\xi) + 1/2)$$

where  $\Phi_0 = h/2e$  is the quantum of flux. In the case of an anisotropic material, this relation remains valid for fields applied along the principal axis. For an applied field along the c-axis, a good approximation of the right hand side parenthesis of the equation can be obtained using the  $\xi$  measurements on LSCO samples of the same composition (10). Using an extrapolation of the  $H_{c1}$  measurements to  $T = 0$ , this gives for our samples a field penetration depth  $\lambda_{\parallel}(T = 0)$  of about 1300 Å.

In this context, the anisotropy is described by the ratio  $\alpha = \frac{\lambda_{\perp}}{\lambda_{\parallel}} = \frac{\xi_{\parallel}}{\xi_{\perp}}$  (25), and can be evaluated to  $2.00 \pm 0.05$ , in agreement with value reported by Zaleski and Klamut (26). In some contrast;  $\lambda_{\parallel}$  at  $T = 0$  was found to be about 2500 Å (10; 25).

Fig. 8 shows the field dependence of the magnetization at  $T/T_c = 0.702$  for both samples, when the field range is extended,  $-4 \times 10^3$  kA/m to  $4 \times 10^3$  kA/m, for applied magnetic fields parallel and perpendicular to the c-axis. A qualitatively similar behavior is seen for the two samples, however with a significantly wider hysteresis loop (higher critical currents) for the sample with the higher critical temperature (sample 2). It is striking to note that there is a crossover field, where the hysteresis loops for the field parallel to the c-axis becomes less wide than for the perpendicular direction. The hysteresis loops in the two directions do in fact show quite different behavior: The “parallel” curves exhibit a minimum at  $H = 0$  followed by a quite sharp maximum after which the magnetization rapidly decreases to become very small at higher fields ( $> 800$  kA/m). The perpendicular hysteresis loops on the other hand shows a sharp maximum at  $H = 0$  followed by a narrow minimum and a broad maximum at a larger field ( $\approx 800$  kA/m) and a slow decrease of the magnetization as the field is further increased. A broad secondary maximum in the magnetization curve have been observed for many different HTS compounds and certain modele have been proposed to explain this (anomalous) behaviour.(27)

As expected for a cuprate superconductor, the anisotropy of the magnetic response is quite remarkable. The system shows a higher first critical field and

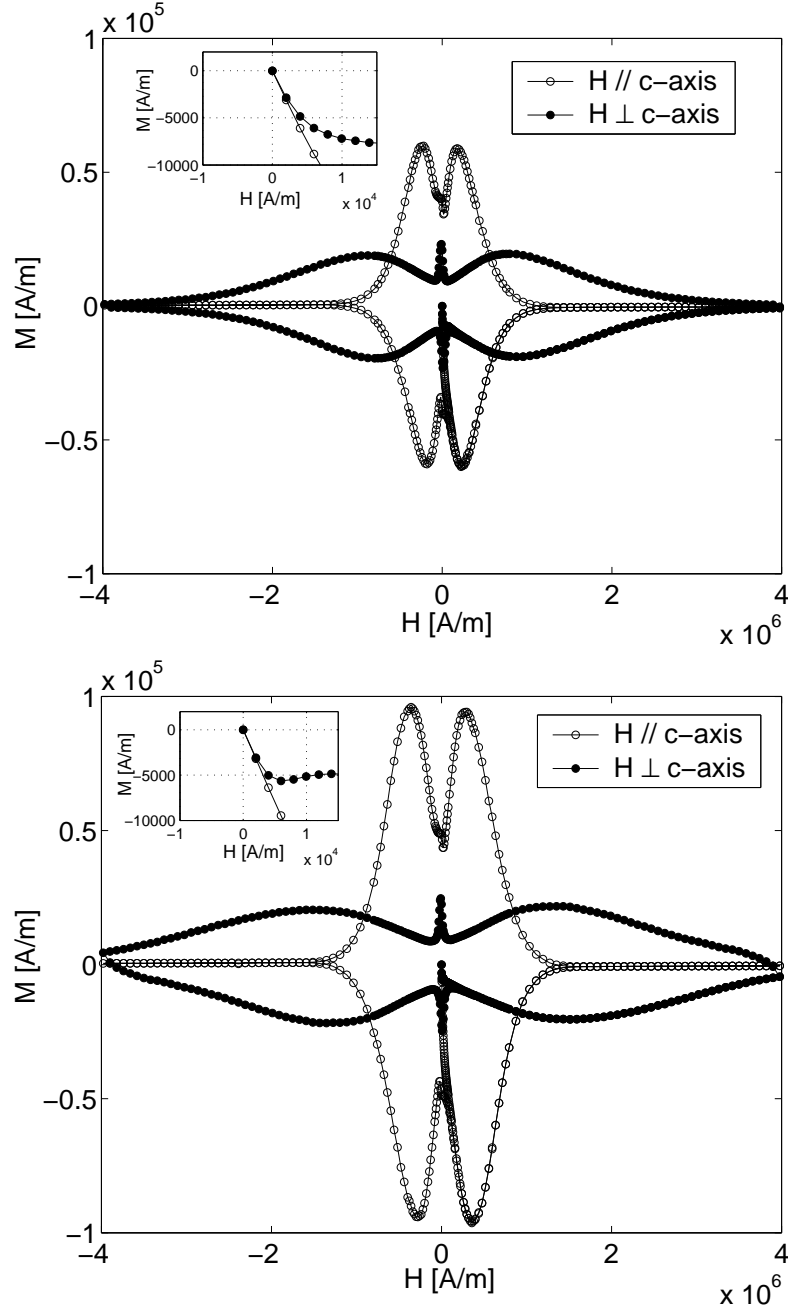


Fig. 8. Field dependence of the magnetization at  $T/T_c = 0.702$  when the field was applied parallel to the  $c$ -axis (open circles) and perpendicular to the  $c$ -axis (solid circles). The inset shows the initial slope for the field dependence of magnetization when magnetic field is applied parallel and perpendicular to the  $c$ -axis. TOP: measured on sample 1; BOTTOM: measured on sample 2.

higher critical currents when the shielding currents can travel only within the  $\text{CuO}_2$ -plane than when they are forced to penetrate the inter-layers. However, at higher magnetic fields, the width of the hysteresis loop, and thus the observed critical currents ( $J_c \propto \Delta M$ ) and the pinning forces become exceedingly

	$H_{m\parallel}$		$H_{m\perp}$	
	$J_{c\parallel}$ (A/m <sup>2</sup> )	$J_{c\perp}$ (A/m <sup>2</sup> )	$J_{c\parallel}$ (A/m <sup>2</sup> )	$J_{c\perp}$ (A/m <sup>2</sup> )
Sample 1	$2.0 \times 10^8$	$4.0 \times 10^7$	$1.5 \times 10^7$	$6.5 \times 10^7$
Sample 2	$3.2 \times 10^8$	$4.0 \times 10^7$	$6 \times 10^5$	$7 \times 10^7$

Table 1

Critical currents evaluated at the different maxima of Fig. 8, i.e.  $H_{m\parallel} \approx 2.2 \times 10^5$  A/m and  $H_{m\perp} \approx 8.7 \times 10^5$  A/m for sample 1 and  $H_{m\parallel} \approx 3.5 \times 10^5$  A/m and  $H_{m\perp} \approx 1.5 \times 10^6$  A/m for sample 2.

larger in the perpendicular than in the parallel configuration. In table 1 the critical current density with the field applied parallel to the c-axis of the sample ( $J_{c\parallel}$ ) and the critical current density with the field perpendicular to the c-axis of the sample ( $J_{c\perp}$ ) are reported. They have been calculated from the magnetization for a full critical state established in a spherical shape sample  $\Delta M = 3\pi J_c a / 16$ , where  $a$  is the sphere radius (28). The shape of the curve and the deduced critical current values show a strong field dependence, which is not taken into account in the critical state model used to evaluate  $J_c$ . However, the results imply a much stronger field dependence of the pinning forces and the flux dynamics when the flux lines penetrate the CuO<sub>2</sub>-planes perpendicularly than when the flux lines are trapped in between the CuO<sub>2</sub>-planes. For the field parallel to the c-axis the current density on the timescale of our experiments, becomes lower than the resolution of our setup, whereas it maintains a considerable magnitude at the corresponding field in the perpendicular direction.

## 4 Conclusions

The magnetic response of two spherical single crystals of LSCO of nominally the same composition, has been found to show qualitatively similar behaviour, although they have somewhat different critical temperatures. At low fields and low temperatures the crystals are perfectly shielding but the field expulsion is weak. The detailed behaviour on approaching the critical temperature shows some significant differences. The sample with the higher critical temperature (sample 2) has a somewhat sharper transition ( $\Delta T_c = 2.6$  K and 2.1 K respectively). On the other hand, the sample with the lower critical temperature shows a wider hysteresis loop in both field directions at the same relative temperature. The anisotropy of the samples can be described by two main features. The first critical field  $H_{c1}$  is found to increase according to an H-dependence on decreasing temperature and to show an anisotropy of about 3.1 independent of temperature. In an anisotropic Ginzburg-Landau Model, it corresponds to an anisotropy of the order parameter coherence length  $\frac{\xi_{\parallel}}{\xi_{\perp}} = 2.0$ . The second aspect concerns irreversibilities. The layered structure of the superconductivity

affects the pinning of the vortices differently in the parallel and perpendicular directions. The critical currents are found to have a stronger field dependence for fields applied along the *c*-axis.

## acknowledgements

P. Svedlindh is acknowledged for helpful discussions, H. Takagi for providing the crystal growth facilities at Takagi Lab., Univ. of Tokyo, P. Mangkorn-tong for crystal growth helping, Håkan Rundlöf for the SXD measurements at Studsvik Neutron Research Laboratory and Nils Olov Ersson for the X-rays measurements.

Financial support from the Swedish Research Council (VR) is acknowledged. A.G. acknowledges the International Science Program of Uppsala University for administrating; the Ministry of Science, Technology and Environment of Thailand for financing a fellowship for research in Sweden. D.H. acknowledges the support of the DYGLAGEMEM European Research Training Network.

## References

- [1] K. Kishio, K. Kitazawa, S. Kanbe, I. Yasuda, N. Sugii, H. Takagi, S. I. Uchida, K. Fueki, S. Tanaka, New High Temperature Superconducting Oxide.  $(\text{La}_{1-x}\text{Sr}_x)_2\text{CuO}_4$  and  $(\text{La}_{1-x}\text{Ca}_x)_2\text{CuO}_4$ , Chem. Lett. 2 (1987) 429–432.
- [2] J. M. Tarascon, L. H. Green, W. R. McKinnon, G. W. Hull, T. H. Geballe, Superconductivity at 40 K in the oxygen-defect perovskites.  $\text{La}_{2-x}\text{Sr}_x\text{CuO}_{4-y}$ , Science 235 (1987) 1373–1376.
- [3] R. B. van Dover, R. J. Cava, B. Batlogg, E. A. Rietman, Composition-dependent superconductivity in  $\text{La}_{2-x}\text{Sr}_x\text{CuO}_{4-\delta}$ , Phys. Rev. B 35 (1987) 5337–5339.
- [4] H. Iwasaki, F. Matsuoka, K. Tanigawa, Magnetization peak around  $H//a$  axis in  $\text{La}_{2-x}\text{Sr}_x\text{CuO}_4$  single crystals with different anisotropy, Phys. Rev. B 59 (1999) 14624–14629.
- [5] T. Sasagawa, Y. Togawa, J. Shimoyama, A. Kapitulnik, K. Kitazawa, K. Kishio, Magnetization and resistivity measurements of the first-order vortex phase transition in  $(\text{La}_{1-x}\text{Sr}_x)_2\text{CuO}_4$ , Phys. Rev. B 61 (2000) 1610.
- [6] T. Tachiki, K. Nakajima, T. Yamashita, I. Tanaka, H. Kojima, Flux Flow of La-Sr-Cu-O Single Crystals, IEEE. Trans. Appl. Supercon. 9 (1999) 2191.
- [7] B. Lake, H. M. Ronnow, N. Chistensen, G. Aeppli, LefmannK., D. F. McMorrow, P. Vorderwisch, P. Smeibidl, N. Mangkorn-tong, T. Sasagawa,

- M. Nohara, H. Takagi, T. E. Mason, Antiferromagnetic order induced by an applied magnetic field in a high-temperature superconductor, *Nature* 415 (2002) 299.
- [8] Y. M. Huh, D. K. Finnemore, Vortex fluctuations in superconducting  $\text{La}_{2-x}\text{Sr}_x\text{CuO}_{4+\delta}$ , *Phys. Rev. B.* 65 (2002) 092506.
- [9] X. Gaojie, P. Qirong, Z. Zengming, D. Zejun, Effect of Oxygen-Deficiency of  $\text{CuO}_2$  Plane on the Structure, Magnetism, and Transport Properties, *Journal of Superconductivity* 14 (2001) 509–517.
- [10] Q. Li, M. Suenaga, Reversible magnetic properties of  $(\text{La}_{1-x}\text{Sr}_x)_2\text{CuO}_4$  single crystals with  $0.05 \leq x \leq 0.10$ , *Phys. Rev. B* 47 (1994) 11384.
- [11] C. A. Durán, P. L. Gammel, R. Wolfe, V. J. Fratello, D. J. Bishop, Direct magneto-optical measurements of anisotropic critical currents in  $(\text{La}_{1-x}\text{Sr}_x)_2\text{CuO}_4$  single crystals, *Phys. Rev. B* 49 (1994) 3608–3612.
- [12] P. Levy, H. Ferrari, C. Acha, V. Bekeris, Irreversibility effects in polycrystalline high- $T_c$  superconductors studied by AC susceptibility, *Physica C* 222 (1994) 212–218.
- [13] L. Leylekian, M. Ocio, M. V. Feigelman, L. B. Ioffe, Glassy superconductor state in  $\text{La}_{1.8}\text{Sr}_{0.2}\text{CuO}_4$  ceramics, *Physica C* 235-240 (1994) 2671–2672.
- [14] H. Maletta, A. P. Malozemoff, D. C. Cronmeyer, C. C. Tsuei, R. L. Greene, J. G. Bednorz, K. A. Müller, Diamagnetic shielding and Meissner effect in the high  $T_c$  superconductor  $\text{Sr}_{0.2}\text{La}_{1.8}\text{CuO}_4$ , *Solid State Commun.* 88 (1993) 837–840.
- [15] R. Decca, R. Isoardi, F. de la Cruz, Linear field dependence of flux flow resistance in high temperature superconductors, *Solid State Commun.* 86 (1993) 103–107.
- [16] A. S. Shcherbakov, V. E. Startsev, E. G. Valiulin, A. N. Petrov, Time dependence of mixed state magnetisation in  $\text{La}_{1.8}\text{Sr}_{0.2}\text{CuO}_4$ , *J. Phys.: Condens. Matter* 2 (1990) 2199–2204.
- [17] L. Leylekian, M. Ocio, J. Hammann, Gauge glass properties in a granular  $\text{La}_{1.8}\text{Sr}_{0.2}\text{CuO}_4$  superconductor, *Physica B* 194–196 (1994) 1865–1866.
- [18] E. Rodríguez, J. Luzuriaga, C. A. D’Ovidio, D. A. Esparza, Softening of the flux-line structure in  $\text{La}_{1.8}\text{Sr}_{0.2}\text{CuO}_4$  measured by a vibrating reed, *Phys. Rev. B* 42 (1990) 10796–10799.
- [19] P. Levy, H. Ferrari, V. Bekeris, C. Acha, AC susceptibility and local intergranular magnetic field in high- $T_c$  superconductors, *Physica C* 214 111–118.
- [20] I. Tanaka, H. Kojima, Superconducting single crystals, *Nature* 337 (1989) 21.
- [21] H. Takagi, T. Ido, S. Ishibashi, M. Uota, S. Uchida, Superconductor-to-nonsuperconductor transition in  $(\text{La}_{1-x}\text{Sr}_x)_2\text{CuO}_4$  as investigated by transport and magnetic measurements, *Phys. Rev. B* 40 (1989) 2254–2261.
- [22] V. Ginzburg, L. Landau, *Zh. Eksp. Teor. Fiz.* 20 (1954) 1064, english translation in *Men of physics: L.D. Landau*, Pergamon (1965).
- [23] J. R. Clem, The Vortex State, Vol. 438 of NATO ASI series C: Mathemat-

- ical and Physical Sciences, Kluwer Academic Publishers, Ch. Anisotropic Superconductors: Fundamentals of Vortices in Layered Superconductors, pp. 25–39.
- [24] C.-R. Hu, Numerical Constants for Isolated Vortices in Superconductors, *Phys. Rev. B* 6 (1972) 1756–1760.
- [25] R. Klemm, J. Clem, Lower critical field of an anisotropic type-II superconductor, *Phys. Rev. B* 21 (1980) 1868.
- [26] A. Zaleski, J. Klamut, Anisotropy of the penetration depth in  $\text{La}_{2-x}\text{Sr}_x\text{CuO}_4$  in underdoped and overdoped regions, *J. Phys.: Condens Matter* 11 (48) (1999) 9731.
- [27] Y. V. Bugoslavsky, A. L. Ivanov, A. A. Minakov, S. I. Vasyurin, Fishtails and anisotropy in underdoped  $\text{LaSrCuO}$  single crystal, *Physica C* 233 (1994) 67–76.
- [28] J. Evetts, A. Campbell, *Concise Encyclopedia of Magnetic & Superconducting Materials*, Pergamon, 1992, Ch. Critical State Model, p. 99.